05952-6183-R000

NAS9-4810

TRW NOTE NO. 67 FMT-303

PROJECT APOLLO
TASK MSC/TRW A-96

ABORT LIMIT LINES DUE TO SATURN V AND APOLLO BLOCK II STRUCTURAL CONSTRAINTS

Prepared by
Structures Department
TRW Systems

3 NOVEMBER 1967

Prepared for
MISSION PLANNING AND ANALYSIS DIVISION
NATIONAL AERONAUTICS AND SPACE ADMINISTRATION
MANNED SPACECRAFT CENTER
HOUSTON, TEXAS

05952-6183-R000

TRW NOTE NO. 67 FMT-303

PROJECT APOLLO
TASK MSC/TRW A-96

ABORT LIMIT LINES DUE TO SATURN V AND APOLLO BLOCK II STRUCTURAL CONSTRAINTS

3 NOVEMBER 1967

Prepared for
MISSION PLANNING AND ANALYSIS DIVISION
NATIONAL AERONAUTICS AND SPACE ADMINISTRATION
MANNED SPACECRAFT CENTER
HOUSTON, TEXAS

Prepared by J.P. Vail
J.R. Vail, Task Manager

Approved by M.E. White
M.E. White, Assistant Manager
Structures Department

Approved by C.R. Coates
C.R. Coates,
Assistant Project Manager
Mission Trajectory Control Program

TRW SYSTEMS GROUP

ABSTRACT

This report is submitted to the NASA Manned Spacecraft Center by TRW Systems in accordance with MSC/TRW Task A-96.6 of the Apollo Mission Trajectory Control Program, Contract NAS 9-4810. The purpose of the report is to present the results of an investigation to establish the feasibility of defining abort limits that may be imposed by the structural constraints of the Saturn V and Apollo Block II spacecraft. In particular, the AS-503 vehicle and mission trajectory were analyzed to evaluate those malfunctions that result in a relatively slow change in vehicle attitude, velocity, position, etc., where it would be expected that the Flight Dynamics Officer could examine the data before making a manual abort decision.

CONTENTS

ILLUSTRATIONS

ILLUSTRATIONS (Continued)

1. INTRODUCTION AND SUMMARY

Abort limits are required to provide the Apollo crew with the maximum available warning time for a safe escape from a malfunctioning launch vehicle system. Both an automatic and manual abort capability are presently programmed for the Apollo missions. The automatic abort is initiated by the emergency detection system (EDS), which is intended for protection from those launch vehicle malfunctions for which there is insufficient crew reaction time. A manual abort is initiated by the crew and provides protection for those malfunctions for which there is sufficient crew reaction time. Both types of aborts require limiting values of specific parameters. These limits may be imposed by various constraints such as launch escape vehicle (LEV) performance, range safety precaution, structural integrity of the system, mission performance, etc.

This study was concerned only with the manual abort limits that may be imposed by the structural constraints and LEV performance constraints of the Saturn V launch vehicle and the Apollo Block II spacecraft during first stage powered flight. The objective of the study was to determine the feasibility of identifying abort limit lines that can be employed for operational monitoring by the Flight Dynamics Officer (FIDO) or possibly by the astronaut. In particular, the AS-503 vehicle and mission trajectory were analyzed to evaluate those malfunctions that result in a relatively slow change in vehicle attitude, velocity, attitude rate, angle of attack, etc., where it would be expected that the FIDO or astronaut could examine the data before making a manual abort decision.

Digital flight simulations were completed for 53 situations in which specific combinations of vehicle malfunctions and altitude winds were considered. Of these simulations, 39 resulted in a structural failure (i.e., loads exceeded the capabilities). However, only the structural failures due to gyro drift malfunctions were easily discernible on the FIDO plotboards.

Analyses of these results revealed that a limit line due to structural constraints could be constructed on the V-γ (inertial velocity versus inertial flight path angle) and the h-d (altitude versus downrange distance) plotboards. This essentially identified "black areas" in which the vehicle would fail structurally.

A flight simulation could not be completed that would result in the vehicle successfully passing into these black areas. This confirmed these black areas as the extreme limits due to structural constraints. The area preceding this black area on each of these plotboards was labeled as a "grey area," since a combination of wind and/or other malfunctions could possibly result in a structural failure.

The gyro drift simulations were further analyzed to determine if the LEV would have sufficient thrust to permit separation during all times of flight. It was found that certain times, characterized by high dynamic pressure at low Mach numbers, would not permit a successful abort. The trajectory data corresponding to these times formed another area on the FIDO plotboards. This area represents a performance limitation; however, no structural constraints are violated by passing through the area.

2. ANALYTICAL APPROACH

A previous TRW study (Reference 1) was conducted to learn the feasibility of determining structural limit lines for the FIDO plotboards. That study had shown that for the Saturn IB/Block I Apollo (AS-204) such lines could be determined for the inertial flight path angle versus inertial velocity (V-γ) plotboard and for the altitude versus downrange distance (h-d) plotboard. Of the many vehicle malfunctions investigated in that study, only very large gyro drift rates (i.e., 0.2 to 1.0 deg/sec) resulted in slowly diverging characteristics that permitted detection on these plots. Other malfunctions, such as engine hardover, loss of attitude reference, etc., had experienced structural failure while still close to the nominal trajectory. In most instances, these rapidly diverging malfunctions would have been detected by the emergency detection system.

It was expected that the results of this AS-503 study would follow the trends established in the Reference 1 study. That is, only the gyro drift malfunctions would provide the slowly divergent trajectories required for determining structural limit lines. The basic approach to the study was to conduct digital flight simulations for the AS-503 vehicle (see Figure 1). Numerous gyro drift malfunctions were simulated to see if they again would provide data for establishing structural limit lines. A limited number of the type malfunctions that had produced rapid divergence for the AS-204 vehicle were also simulated to verify that the same results were obtained for the AS-503 vehicle.

The TRW N-stage digital simulation program was employed for the trajectory simulations. This program, described in more detail in Reference 1, considers the overall vehicle as a rigid body system. The structural loads normally computed by this program therefore only reflect a rigid body vehicle. However, dynamic load factors were inserted into the load equations to account for any additional loads due to flexible body considerations. Thus, the computed time histories of structural loads reflected a flexible body system.

Although many digital flight simulations were conducted in this investigation, only two basic inputs were varied for each simulation: notably, the vehicle malfunction and the wind environment the vehicle encounters. These two inputs to the program are identified and discussed in the following sections.

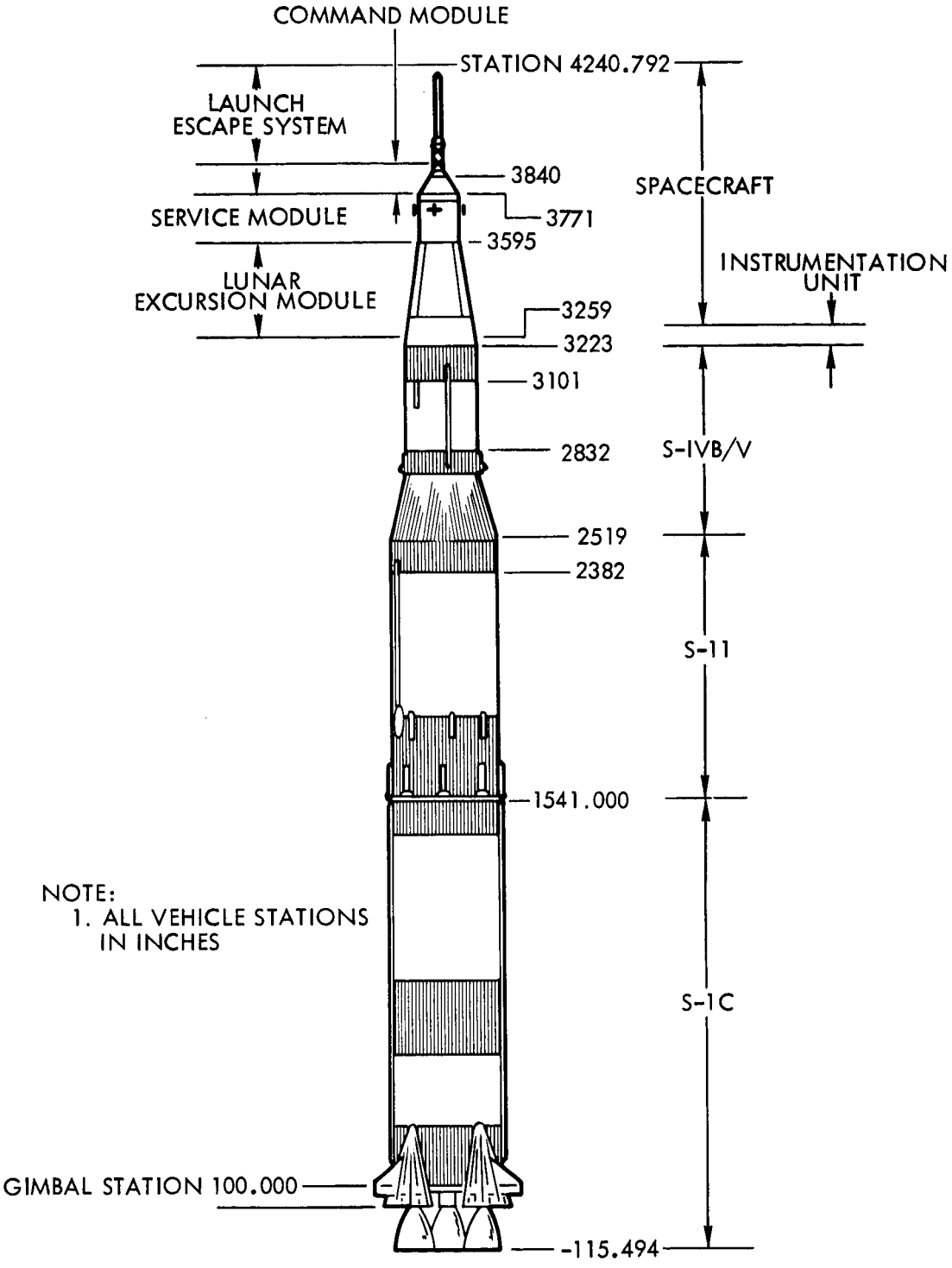

Figure 1. Apollo/Saturn V Vehicle

2.1 MALFUNCTIONS

There are many malfunctions that the Saturn V launch vehicle could experience during its first stage flight. Reference 2 identifies several of these malfunctions that could lead to structural failures for the Saturn V and associates a criticality number with each to indicate its relative probability of occurrence. (The higher the criticality number, the more likely a loss of the mission.) From this listing, the following were selected for evaluation in this study. (The gyro drift malfunction was not listed in Reference 2)

a. Loss of pitch inertial attitude reference
b. Loss of pitch attitude error signal
c. Saturated pitch attitude error signal
d. Engine hardover
e. Engine out
f. Pitch down gyro drift

The above malfunctions can occur at any time during first stage flight and can have various magnitudes, direction, degrees, etc. Thus, as can be visualized, a multitude of malfunction conditions can be conceived. However, since it was only desired to verify previous results, only a limited number of each of the types of malfunction simulations were made. Generally, the malfunction was selected to result in an increased structural load environment. For example, gyro drift malfunctions were selected to pitch the vehicle down and encounter a more severe dynamic pressure environment. The Reference 1 study had shown that it was not feasible to establish yaw plane (i.e., crossrange) structural limit lines. Yaw plane malfunctions were therefore not investigated in this study. Finally, note that no consideration was given to multiple malfunctions (i.e., the occurrence of more than one malfunction on a single trajectory simulation).

The simulations of the engine out malfunction employed the "chi-freeze" procedure (Reference 2). Once an engine has failed, the commanded pitch (chi) signal is held constant for a specified length of time. At the end of this chi-freeze period, the commanded pitch program is resumed. Thus, the continued pitch program is delayed by a time increment equal to the chi-freeze period, which is dependent upon the time of flight at which the engine failed.

2.2 ALTITUDE WINDS

The altitude winds have a significant effect on the flight and performance of any launch vehicle. In particular, the winds provide flight disturbances, which in turn induce structural loads on the vehicle. Thus, the establishment of any abort limit lines due to structural constraints must consider the influence of altitude winds.

The structural design of both the Saturn launch vehicle and Apollo spacecraft was based on the use of "synthetic" wind profiles to represent the anticipated wind environment. Essentially, this involves the synthesis of a single wind profile on the basis of statistics of measured wind velocity and wind shears at various altitudes. These design wind profiles (Reference 3) were constructed from scalar winds (i. e., with no regard to a specific direction) and were applied as either a headwind, tailwind, or crosswind to derive the most severe loads (Figure 2).

For this particular investigation, directional wind profiles (i. e., winds based on components for the intended launch azimuth) were primarily employed, since they provided a more realistic representation of the altitude winds (Reference 3).

The wind environment was considered in the malfunction trajectories for two primary reasons. Certain malfunctions did not affect the vehicle sufficiently to induce structural failures in the absence of winds. Winds were therefore used with these malfunctions to provide an additional disturbance in an attempt to induce failure cases. The second use of wind profiles was in evaluating the maximum change, which could be produced in various plotboard parameters at the time of structural failure. This provided an indication of the uncertainty that would have to be associated with any limit lines identified.

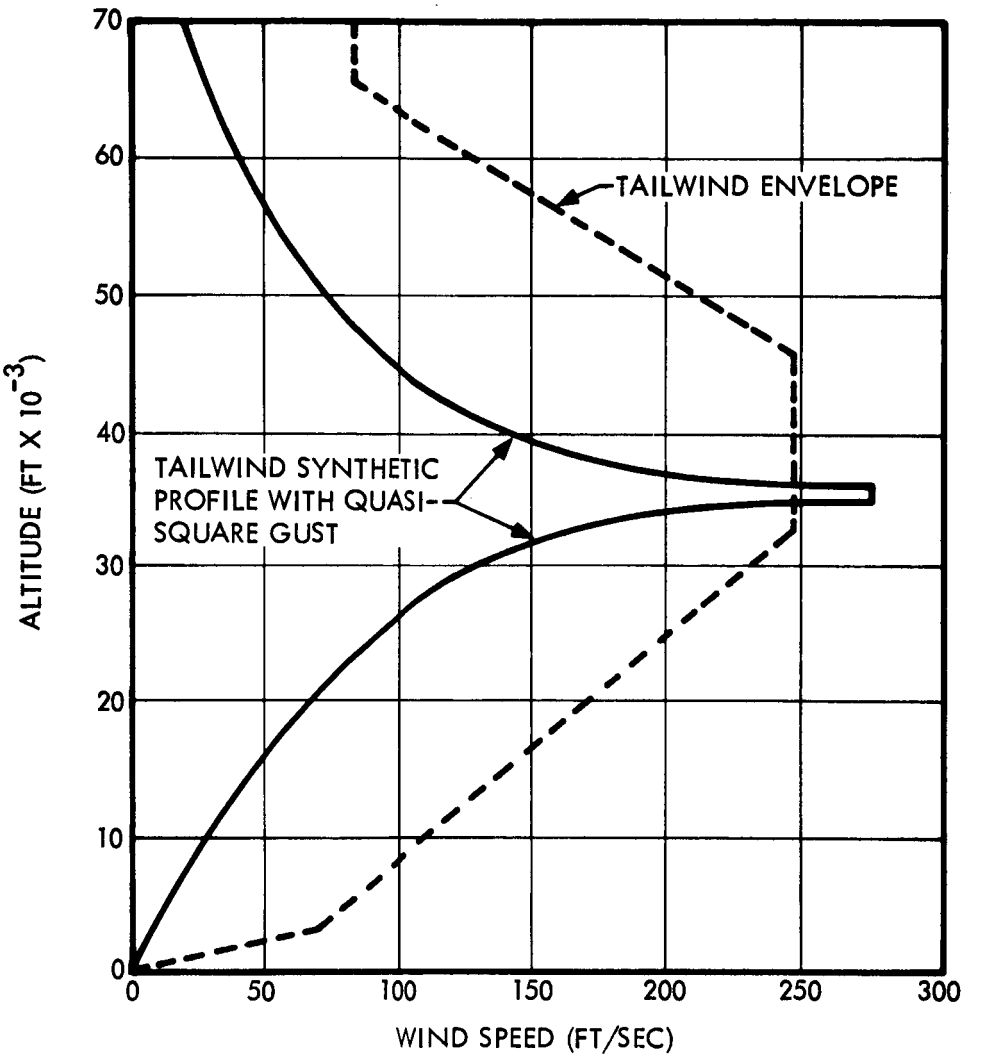

Figure 2. Illustration of Altitude Wind Criteria

3. VEHICLE AND TRAJECTORY DATA

The AS-503 vehicle and mission trajectory were employed as the baseline for this investigation. The following sections identify the data that were employed or make reference to NASA reports from which data were extracted.

3.1 MASS PROPERTIES

The mass properties for use in the trajectory response determination were obtained from Reference 4. Mass distributions for the structural load calculations were extracted from References 4, 5, and 6.

3.2 AERODYNAMIC STABILITY CHARACTERISTICS

The aerodynamic normal force, center of pressure, and drag coefficients at all Mach numbers during first stage flight were obtained from Reference 7.

3.3 AERODYNAMIC LOAD DISTRIBUTIONS

The aerodynamic normal force and drag distribution along the vehicle longitudinal axis were derived from the data of Reference 8. This particular document utilizes wind tunnel data from several tests and configurations and correlates them into a single set of data for the AS-503 configuration.

3.4 SATURN V CONTROL SYSTEM

The definition of the Saturn V control system for this study was previously documented in Reference 9 along with an identification of the NASA/MSFC documents from which it was derived. Revised control gains and filter coefficients were obtained from Reference 10. Block diagrams of the control system model were presented in Reference 1.

3.5 ATMOSPHERIC PROPERTIES

Reference 11 was employed to obtain the atmospheric properties for the flight simulation at the Cape Kennedy launch site.

3.6 TRAJECTORY

The AS-503 nominal trajectory and associated parameters were extracted from Reference 12. The use of a dispersed maximum dynamic

pressure trajectory would have provided a more severe structural loading environment and resulted in earlier failures for the rapidly diverging malfunctions. The slowly diverging gyro drift malfunctions, which induce dynamic pressures 200 to 300 percent higher than nominal, would not be noticeably affected by the 6 percent increase in dynamic pressure provided by a dispersed trajectory.

3.7 PROPULSION

The vehicle thrust, as a function of altitude, was obtained from Reference 12 and employed in the digital flight simulations.

3.8 CRITICAL VEHICLE STATIONS

Structural loads (i.e., shear, bending moment and axial load) were computed on a time history basis for the vehicle stations identified below and shown on Figure 1. These critical stations were selected on the basis of the minutes of various MSFC/MSC panel meetings and from informal discussions with NASA personnel.

Number	Saturn Station	Description
1	3840	LES/CM interface
2	3771	CM/SM
3	3595	SM/SLA
4	3529	SLA/IU
5	3223	IU/S-IVB
6	3101	Forward Y-joint of S-IVB
7	2832	Aft Y-joint of S-IVB
8	2519	Separation point of S-IVB/S-II
9	2382	Forward Y-joint of S-II
10	1541	Separation point of S-II/S-IC

3.9 STRUCTURAL CAPABILITIES

As specified in the task agreement, ultimate capability values were considered in determining structural failures. The spacecraft structural capabilities were obtained from Reference 13. The launch vehicle capabilities were obtained from Reference 14 and modified to account for the increased tension allowables presented in Reference 15. The capabilities at room temperature were considered in this study for the following reasons:

a. The critical loads are practically always experienced before the aerodynamic heating induces sufficient temperatures to degrade the structural capabilities.

b. The determination of the temperature time profile at various vehicle stations was not in the scope of this task.

c. The existing capability data for elevated temperatures is incomplete (e. g., data for only two stations and for one temperature level).

3.10 DYNAMIC LOAD FACTORS

Since the digital flight simulations were conducted on a rigid body basis, the resulting rigid body loads were multiplied by dynamic load factors to account for additional loads due to flexible body considerations. These factors, which are presented in Figure 3, were obtained from MSFC personnel (Reference 16).

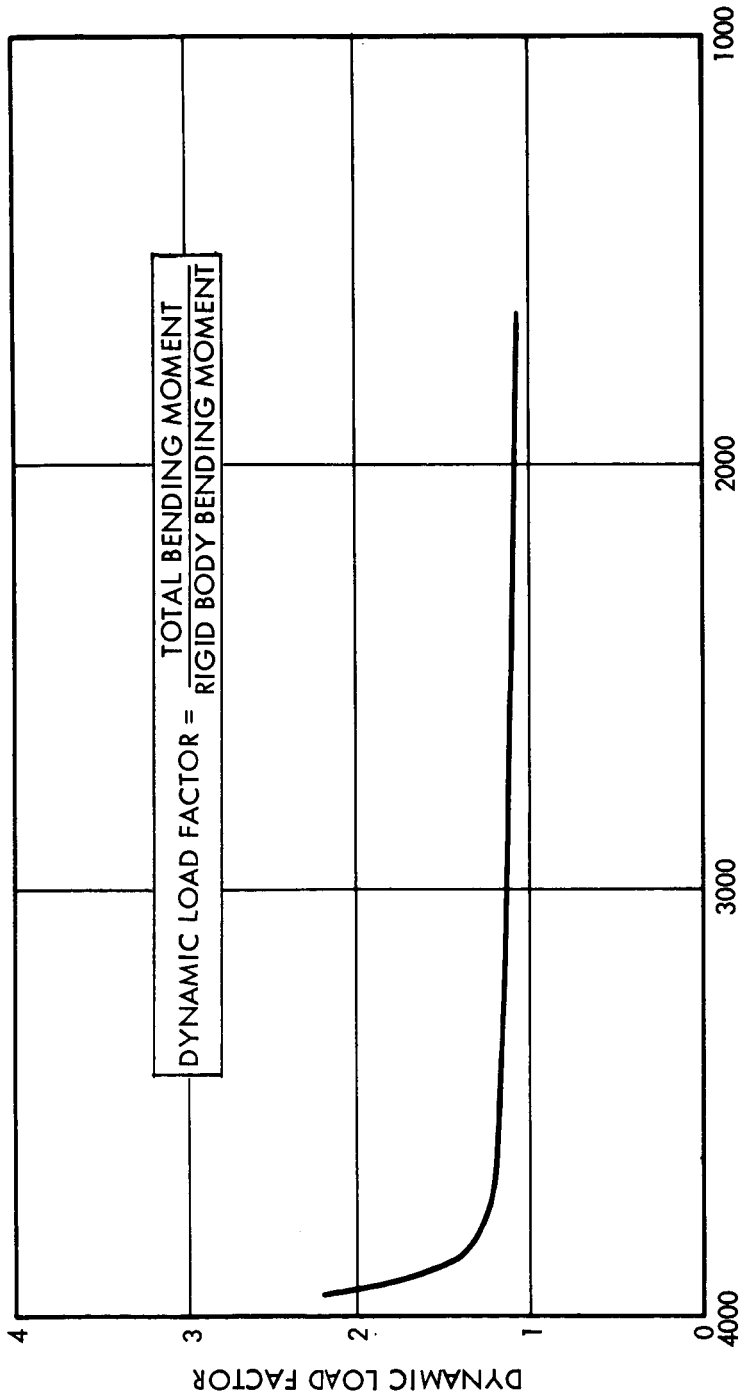

Figure 3. Dynamic Load Factors for the AS-503 Vehicle

4. SIMULATIONS

It would be possible to simulate an almost unlimited number of combinations of vehicle malfunctions and altitude wind conditions. However, as stated in the analytical approach to this study (Section 2), it was primarily desired to verify that the trends established for the AS-204 vehicle would remain the same for the AS-503 vehicle. In view of this, only those malfunctions that were known to lead to Saturn V structural failures were simulated.

The data presented in Reference 2 was the basis for selecting malfunctions that could lead to structural failure. This reference also identified the magnitude and direction of the winds that were required to induce structural failures for specific malfunctions. The altitude at which the peak wind velocity occurs must also be phased in many instances. The determination of this critical phasing can again require a large number of simulations. For this study, the required winds were peaked initially at 33,000 feet. If this did not induce a failure, the wind magnitude was increased from the directional wind speed to the scalar wind speed. If a failure still was not obtained, the altitude of the peak wind was then varied to find the proper phasing.

A summary of the particular simulations completed in this study is presented in Table 1. This table identifies (1) the malfunction, (2) its time of occurrence, (3) its magnitude, degree, direction etc., and (4) the wind environment considered.

Table 1. Log of Trajectory Simulations for Saturn V/Block II Malfunctions

Case Number	Description	Failure Cases
	No Malfunction Conditions	
1	Nominal	no
2	Nominal, 95 tailwind, peak at 35K ft	no
3	Nominal, 95 scalar wind, 7° Az, peak at 33K ft	no
	Loss of Pitch Inertial Attitude Reference Conditions	
4	At 40 sec, holding last attitude error signal	yes
5	At 60 sec, holding last attitude error signal	yes
6	At 60 sec, w/o holding last attitude error	yes
7	At 80 sec, holding last attitude error signal	no
8	At 95 sec, holding last attitude error signal	no
9	At 105 sec, holding last attitude error signal	no
	Loss of Pitch Attitude Error Signal Conditions	
10	At 60 sec	yes
11	At 70 sec	yes
	Saturated Pitch Attitude Error Signal Conditions	
12	At 40 sec	yes
13	At 60 sec	yes
14	At 80 sec	yes
15	At 95 sec	yes
16	At 105 sec	yes
	Engine Hardover Conditions	
17	No. 1 right at 65 sec, 95% lft qtr headwind, peak at 33K ft	no
18	No. 1 right at 65 sec, 95% scalar wind, peak at 33K ft	yes
19	No. 1 right at 75 sec, 95% lft qtr headwind, peak at 33K ft	no
20	No. 1 right at 75 sec, 95% scalar wind, peak at 33K ft	no
21	No. 1 right at 75 sec, 95% lft qtr headwind, peak at 45K ft	yes
	Engine Out Conditions	
22	No. 2 out at 65 sec, 95% lft qtr headwind, peak at 33K ft	no
23	No. 2 out at 75 sec, 95% scalar wind, peak at 33K ft	no
24	No. 2 out at 75 sec, 95% lft qtr headwind, peak at 33K ft	no
	Pitch Down Gyro Drift Conditions	
25	0.17 deg/sec at lift-off	no
26	0.20 deg/sec at lift-off	no
27	0.25 deg/sec at lift-off	yes
28	0.30 deg/sec at lift-off	yes
29	0.35 deg/sec at lift-off	yes
30	0.50 deg/sec at lift-off	yes
31	0.75 deg/sec at lift-off	yes
32	1.00 deg/sec at lift-off	yes
33	0.5 deg/sec at 30 sec	yes
34	0.5 deg/sec at 40 sec	yes
35	0.5 deg/sec at 50 sec	yes
36	0.5 deg/sec at 60 sec	yes
37	0.75 deg/sec at 30 sec	yes
38	0.75 deg/sec at 40 sec	yes
39	0.75 deg/sec at 45 sec	yes
40	0.75 deg/sec at 50 sec	yes
41	0.75 deg/sec at 60 sec	yes
42	0.75 deg/sec at 70 sec	yes
43	1.00 deg/sec at 40 sec	yes
44	1.00 deg/sec at 60 sec	yes
45	1.00 deg/sec at 70 sec	yes
46	1.00 deg/sec at 80 sec	yes
47	1.25 deg/sec at 75 sec	yes
48	1.25 deg/sec at 80 sec	yes
49	1.30 deg/sec at 80 sec	yes
50	0.50 deg/sec at liftoff, 99% headwind, peak at 33K ft	yes
51	0.50 deg/sec at 40 sec, 99% headwind, peak at 33K ft	yes
52	0.50 deg/sec at liftoff, 95% tailwind, peak at 33K ft	yes
53	0.50 deg/sec at 40 sec, 95% tailwind, peak at 33K ft	yes

5. ANALYSIS OF RESULTS

Of the 53 simulations that were conducted, 39 resulted in a structural failure. A summary of these particular failure cases is presented in Table 2. For each such case, the time of failure is identified along with the associated performance parameters related to the FIDO plotboards. These results are illustrated in Figures 4 and 5 in which the points of failure, according to their type of malfunction, are noted on the V-γ and h-d FIDO plotboards. The baseline trajectory is also identified on Figures 4 and 5 for reference purposes.

It may be observed from Figures 4 and 5 that all malfunctions other than the gyro drifts resulted in negligible changes in the vehicle trajectory up to the time of structural failure. The primary effect of the these other malfunctions was to rapidly induce large angles of attack, which in turn induced large loads. This resulted in structural failures at close to nominal trajectory values. It is obviously not feasible to construct abort limit lines on the FIDO displays for these malfunctions. The gyro drifts, however, slowly depressed the trajectory into the denser atmosphere while maintaining relatively small angles of attack. The depressing of the trajectory induced very high dynamic pressures and therefore large loads at quite off-nominal trajectory conditions.

The engine-out and engine hardover conditions are interesting in that they are both quite wind dependent. Several simulations with varying wind conditions were required to obtain a structural failure for the engine hardover condition. A failure was not obtained for the single engine out condition with chi-freeze. However, it was noted that loss of one engine did not significantly effect the trajectory parameters. Determining the phasing of engine-out time with altitude of the peak wind velocity would result in a failure close to the nominal trajectory.

As observed in Figures 4 and 5, the pitch plane gyro drift malfunctions resulted in considerable deviations from the intended trajectory. The results of these particular malfunctions were therefore analyzed separately and in more detail. These analyses are discussed in the following sections.

Table 2. FIDO Plotboard Parameters at Time of Structural Failure

Case No.	Time of Failure (sec)	*Station Failed	Inertial Velocity (ft/sec)	Inertial Attitude (deg)	Downrange Distance (n. mi.)	Altitude (n. mi.)
4	86.4	6	3143	25.50	4.60	8.88
5	92.6	6	3476	24.80	6.11	10.50
6	63.9	4	2097	27.75	1.14	4.38
10	79.1	6	2589	33.41	2.87	7.40
11	85.7	6	2937	32.86	4.17	8.90
12	45.8	4	1664	19.96	0.24	1.98
13	63.9	6	2097	27.75	1.14	4.38
14	83.7	7	2925	28.82	3.84	8.36
15	99.8	7	3880	26.46	8.21	12.72
16	108.0	1	4502	27.08	11.41	15.37
18	69.4	6	2275	29.48	1.63	5.35
20	82.8	6	2904	28.39	3.75	8.12
27	124.0	2	6615	2.81	29.44	12.67
28	100.0	2	4518	9.12	14.06	9.23
29	89.8	2	3857	10.84	10.06	7.42
30	78.8	2	3361	9.26	7.48	5.20
31	70.0	2	3124	4.94	6.34	3.41
32	63.6	2	2987	1.32	2.32	5.59
33	96.0	2	4108	9.60	10.29	8.88
34	108.0	6	4946	6.86	15.28	11.23
35	126.0	6	6576	1.08	26.90	14.06
36	148.0	6	9059	-3.66	48.80	16.82
37	78.0	6	3056	12.89	4.71	5.89
38	82.0	6	3150	14.96	4.89	6.95
39	86.0	6	3334	14.77	5.67	7.80
40	94.0	6	3816	11.98	8.07	9.28
41	108.0	6	4792	8.45	13.76	12.27
42	130.0	6	6814	0.21	28.43	16.16
43	71.8	6	2630	18.08	2.72	5.33
44	80.0	6	2837	23.40	3.38	7.31
45	108.0	6	4695	9.76	13.04	12.93
46	134.0	6	7101	-1.73	30.99	17.48
47	108.0	6	4631	9.99	12.71	13.22
48	122	6	5774	2.17	20.99	15.79
49	108	6	4588	14.28	12.25	14.03
50	78	2	3424	8.62	7.85	5.33
51	108	6	4928	6.98	15.13	11.30
52	80	2	3465	8.14	8.05	5.23
53	108	6	4988	6.60	15.67	11.06

*Refer to Section 3.8 for description of station.

5.1 PITCH PLANE GYRO DRIFTS

The primary purpose of this study was to determine structural limit lines that could be placed on the FIDO plotboards to warn of approaching structural failure. The V-γ and h-d history of each no-wind gyro drift trajectory were therefore plotted to determine if an area could be determined where a structural failure would occur. These plotboard histories are shown in Figures 6 through 15 for various drift rate initiation times.

Each of the drift initiation times resulted in a distinct structural limit line being formed. These lines are also shown on Figures 6 through 15. If the only possible malfunction during an actual flight was a constant gyro drift, and if the rate and time of initiation of that drift could be determined, each of these lines could be used as a basis for abort decisions. Unfortunately, this is not the case. Using the limit line closest to the nominal trajectory would result in aborts sooner than would be required for most of the cases simulated. For example, the 0.20 deg/sec case (initiated at lift-off) would be aborted, when, in reality, structural failure did not occur.

The only structural limit line that can be formed, where a high probability of failure exists for all no-wind cases, is the inner envelope of the four individual lines. This is shown in Figures 16 and 17. Obviously, many failures could occur outside of these lines. However, a no-wind trajectory could not be found that would penetrate the lines without structural failure.

The effects of altitude winds on the structural limit lines were evaluated by simulating two drift rates with 99 percent headwind and 95 percent tailwind profiles. The failure points for these cases are shown on Figures 7 and 12, where they may be compared with the no-wind cases. Both cases of a 0.5 deg/sec drift rate initiated at lift-off are seen to fail slightly later than the no-wind case. The same drift rate initiated at 40 seconds fails slightly earlier with a head wind and slightly later with a tailwind. Based on these results, it was concluded that an extensive investigation would be required to determine the full effect of all possible wind profiles on the limit lines. However, it is felt that such a study would only result in minor shifting of the no-wind limit line and is not really warranted.

Another trajectory is noted on Figures 4 and 5 for reference purposes only. This trajectory resulted from a pitch down gyro drift malfunction. Although it did not result in a structural failure, its aerodynamic heating indicator $\left(\int qVdt\right)$ reached a value of 2.09×10^6 lb/ft at the end of first stage flight. The value slightly exceeds the Saturn V Block I (AS-501) design aerodynamic heating trajectory ADH of 2.03×10^6 lb/ft (Reference 17). The AS-503 design aerodynamic heating indicator is not known.

5.2 LEV SEPARATION LIMITS

Reference 18 presented the results of a TRW study to determine the limiting conditions for short term separation of the launch escape vehicle (LEV) from the Saturn V launch vehicles (LV). These limiting conditions were presented as tables of combinations of Mach number (M), dynamic pressure (q), and altitude and velocity (air speed) for various values of LEV and LV weight and thrust. These parameters described conditions for which the LEV thrust was not sufficient to overcome the aerodynamic drag on the LEV. Separation therefore could not be achieved. The trajectory parameters from the gyro drift trajectories of this study were combined with those results to determine if the LEV limiting conditions were exceeded.

Figure 18 shows the limiting Mach number - dynamic pressure (M-q) conditions from Reference 18. The actual M-q combinations from the gyro drift trajectories, which exceeded these limiting conditions, are also shown. The trajectory V-γ and h-d values corresponding to the intersection of the limiting and actual M-q values for the drift rates initiated at "lift-off" were determined to form the LEV separation limitation line shown on Figures 6 and 11. Only one of the "delayed" gyro drift cases (Case 37) intersected the limiting M-q line. The combined LEV separation limitation lines resulting from this case and the lift-off initiated drift conditions are shown on Figures 16 and 17.

6. CONCLUSION AND RECOMMENDATIONS

Of the 53 malfunction simulations conducted in this investigation, 39 resulted in structural failure. Of these failure cases, only the gyro drifts in the pitch planes resulted in considerable deviation from the intended trajectory and were reflected on the FIDO plotboards.

Analyses of the pitch plane gyro drift cases revealed that a limit line due to structural constraints could be constructed on the V-γ and h-d FIDO plotboards. This essentially identified black areas in which the vehicle would fail structurally. A flight simulation could not be completed that would result in the vehicle successfully passing into this black area. This confirmed the black area as the extreme limit due to structural constraints. The area preceding this black area was labeled as a grey area, since a combination of winds and/or other malfunctions could possibly result in a structural failure.

Similarly, an area was defined on the V-γ and h-d plotboards where the LEV probably cannot separate from the LV during an abort sequence. Again, cases were found where separation could not occur outside of this area. However, a case was not found where separation could occur within the area.

It was noted that one fairly low gyro drift rate trajectory exceeded a "design" aerodynamic heating indicator value prior to structural failure. This study did not consider the effects of elevated temperatures on structural capabilities and, in turn, on the position of the structural limit lines. It is therefore recommended that such an analysis be performed.

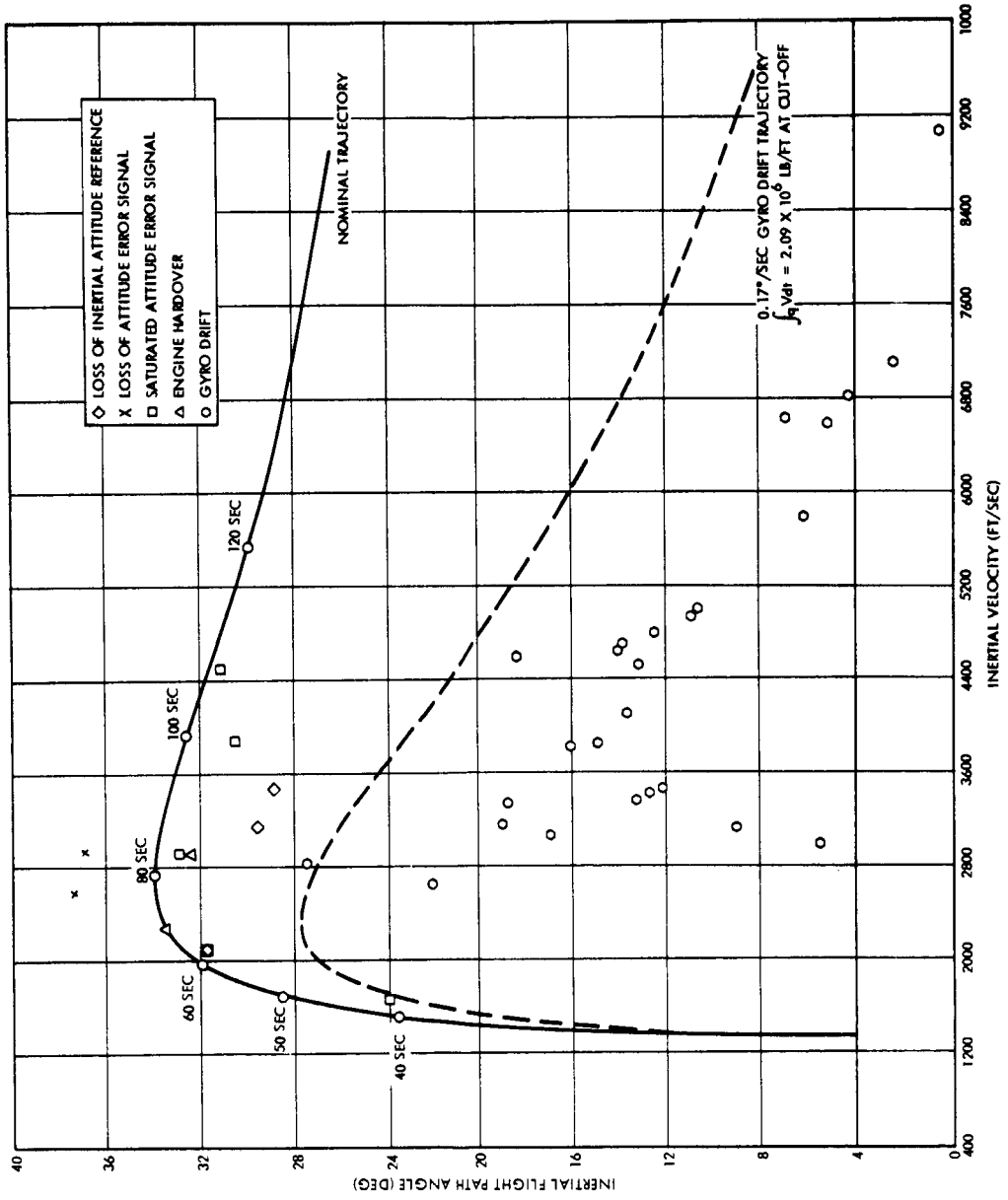

Figure 4. AS-503 Summary of Failure Points on Inertial Attitude Versus Inertial Velocity Plotboard

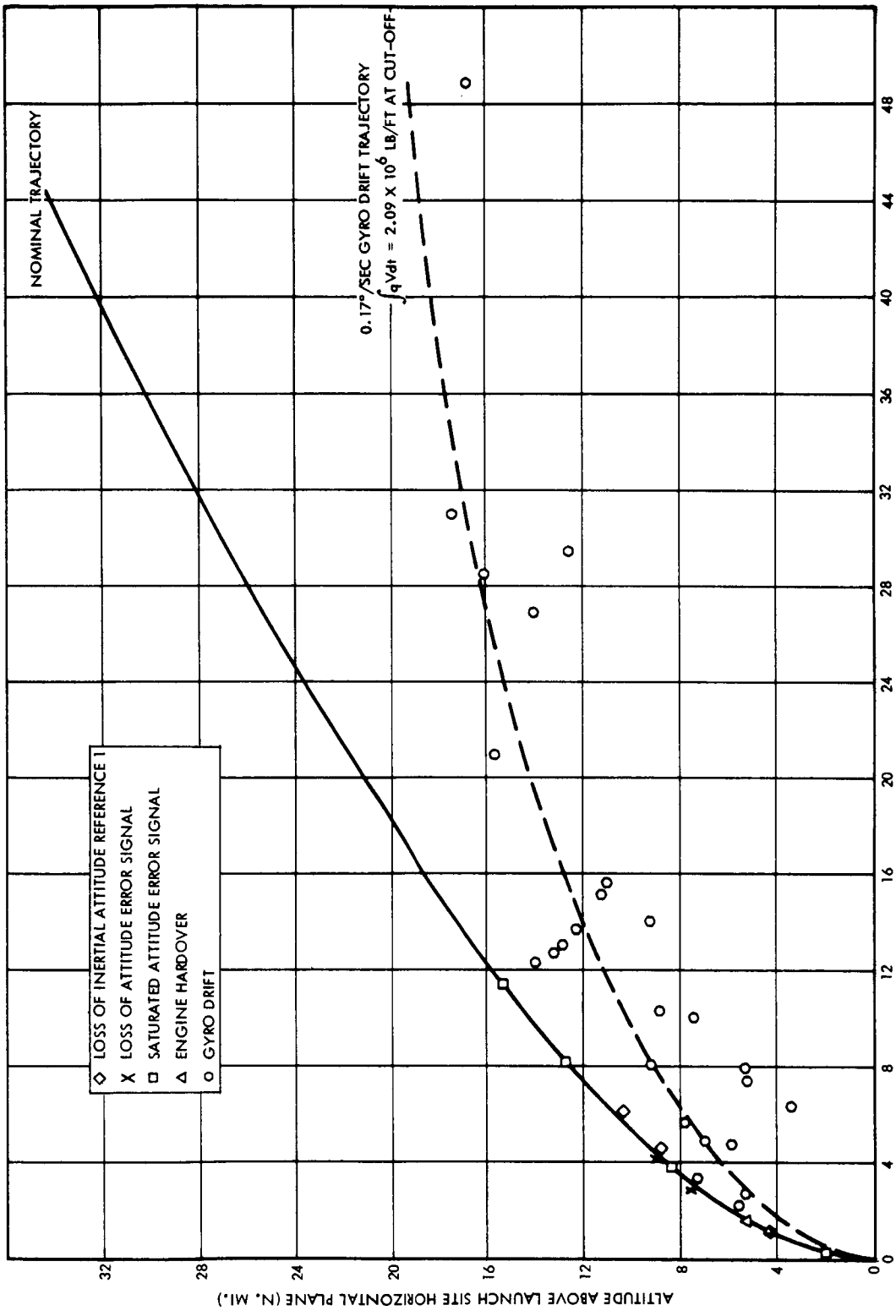

Figure 5. AS-503 Summary of Failure Points on Altitude Versus Downrange Distance Plotboard

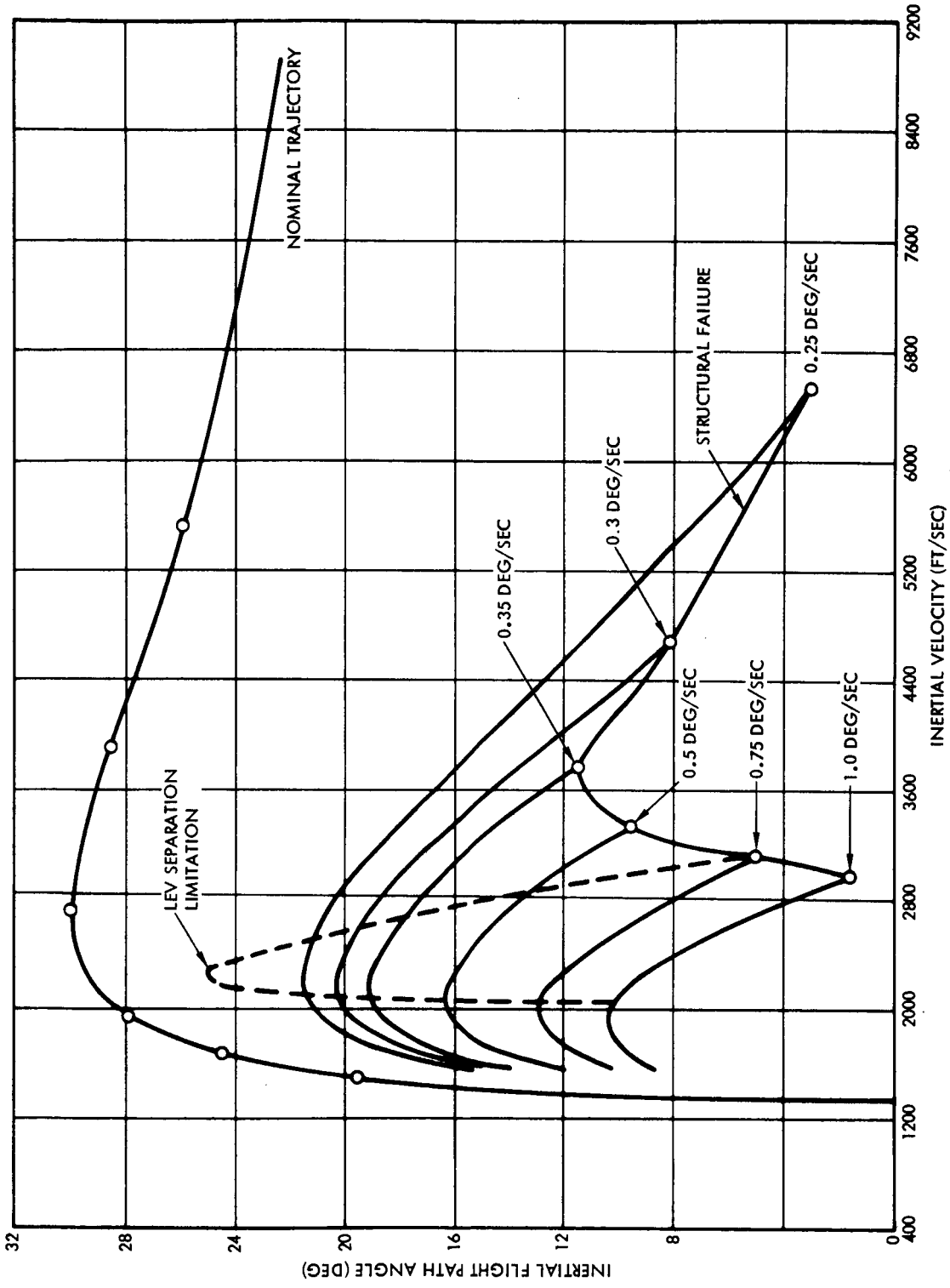

Figure 6. AS-503 Malfunctioning Gyro Trajectories Constant Pitch Down Drift Rates Initiated at Lift-off

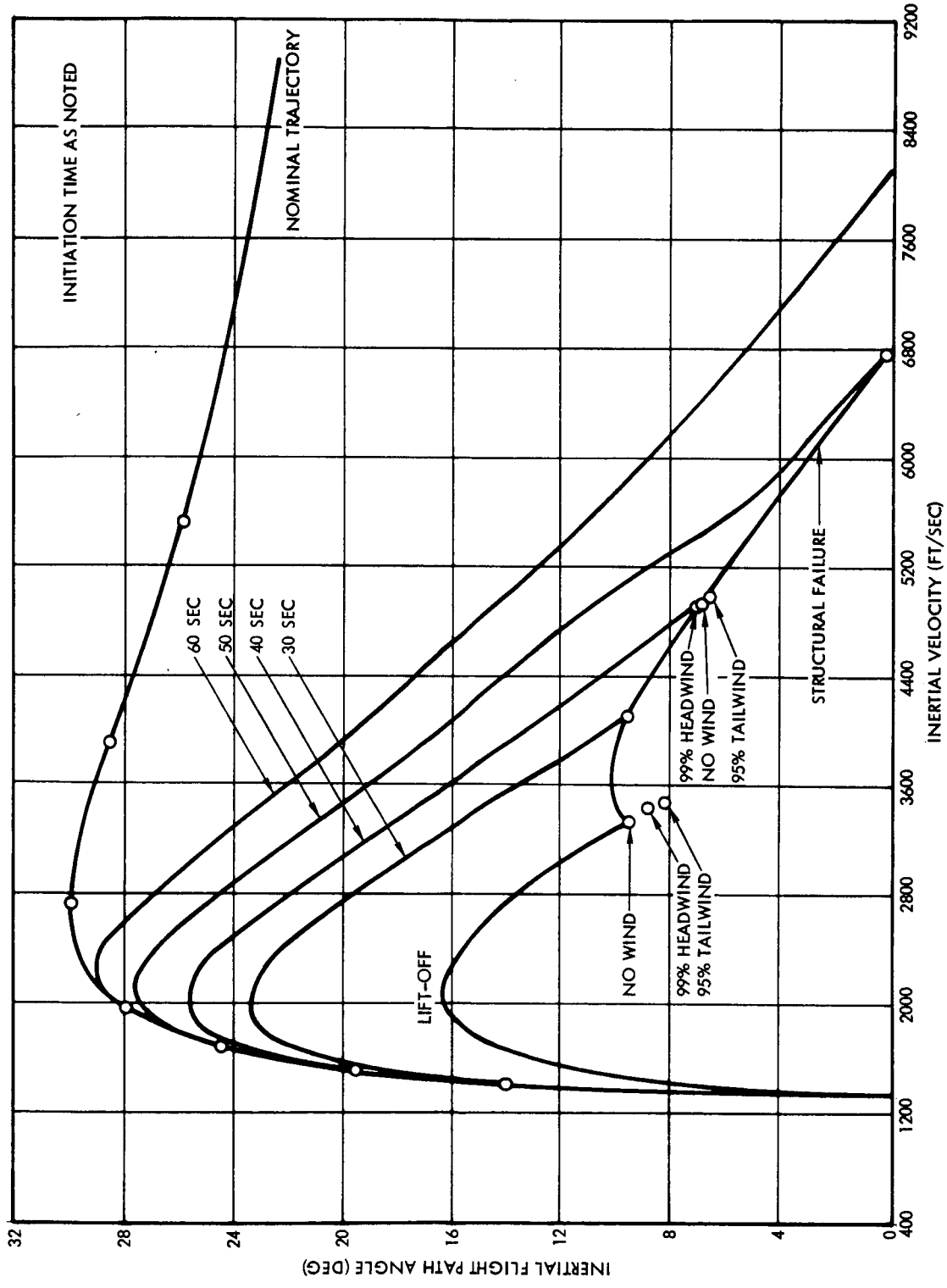

Figure 7. AS-503 Malfunctioning Gyro Trajectories, Constant 0.5 deg/sec Pitch Down Rate with Delayed Initiation Times

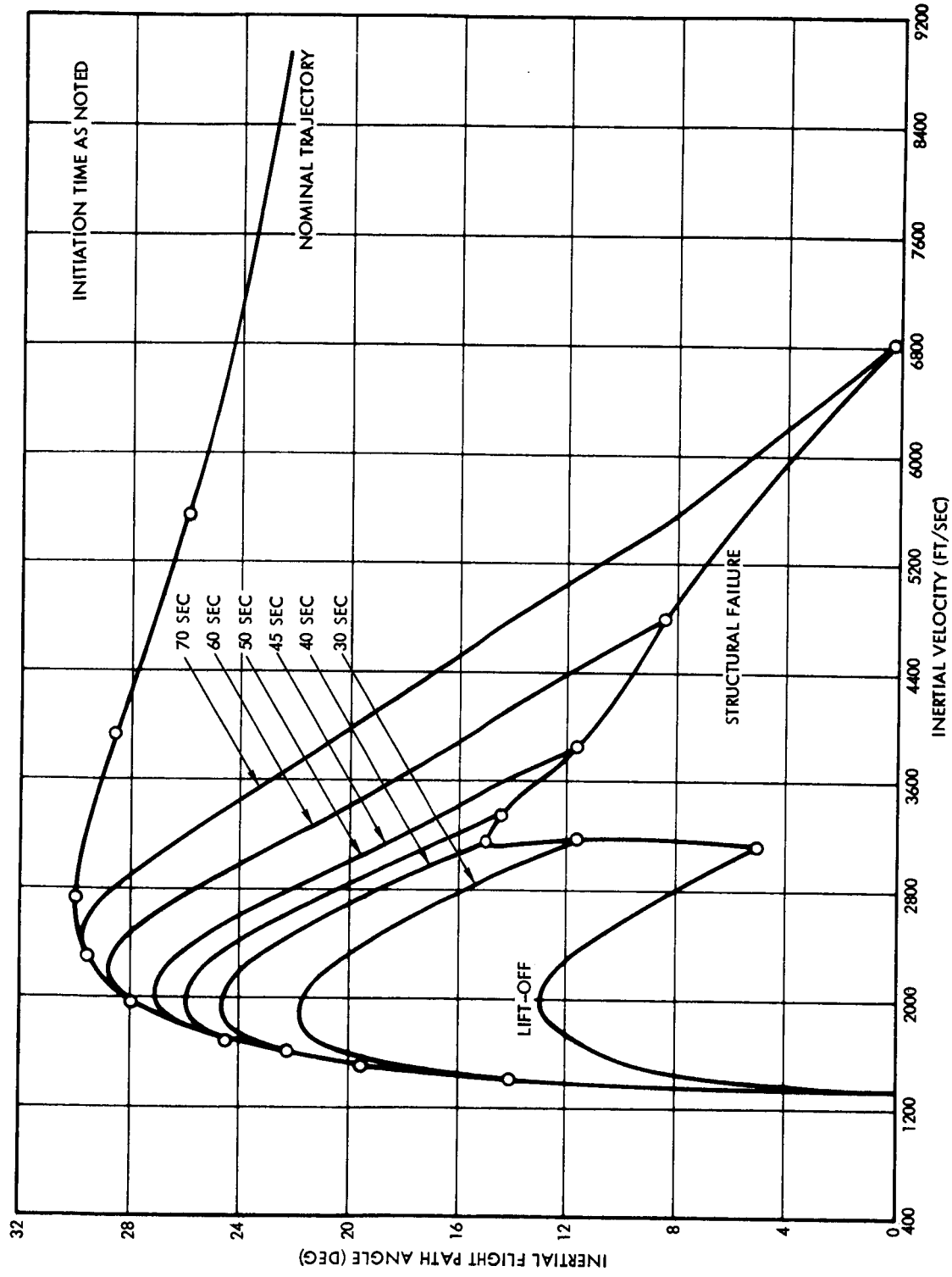

Figure 8. AS-503 Malfunctioning Gyro Trajectories, Constant 0.75 deg/sec Pitch Down Drift Rate with Delayed Initiation Times

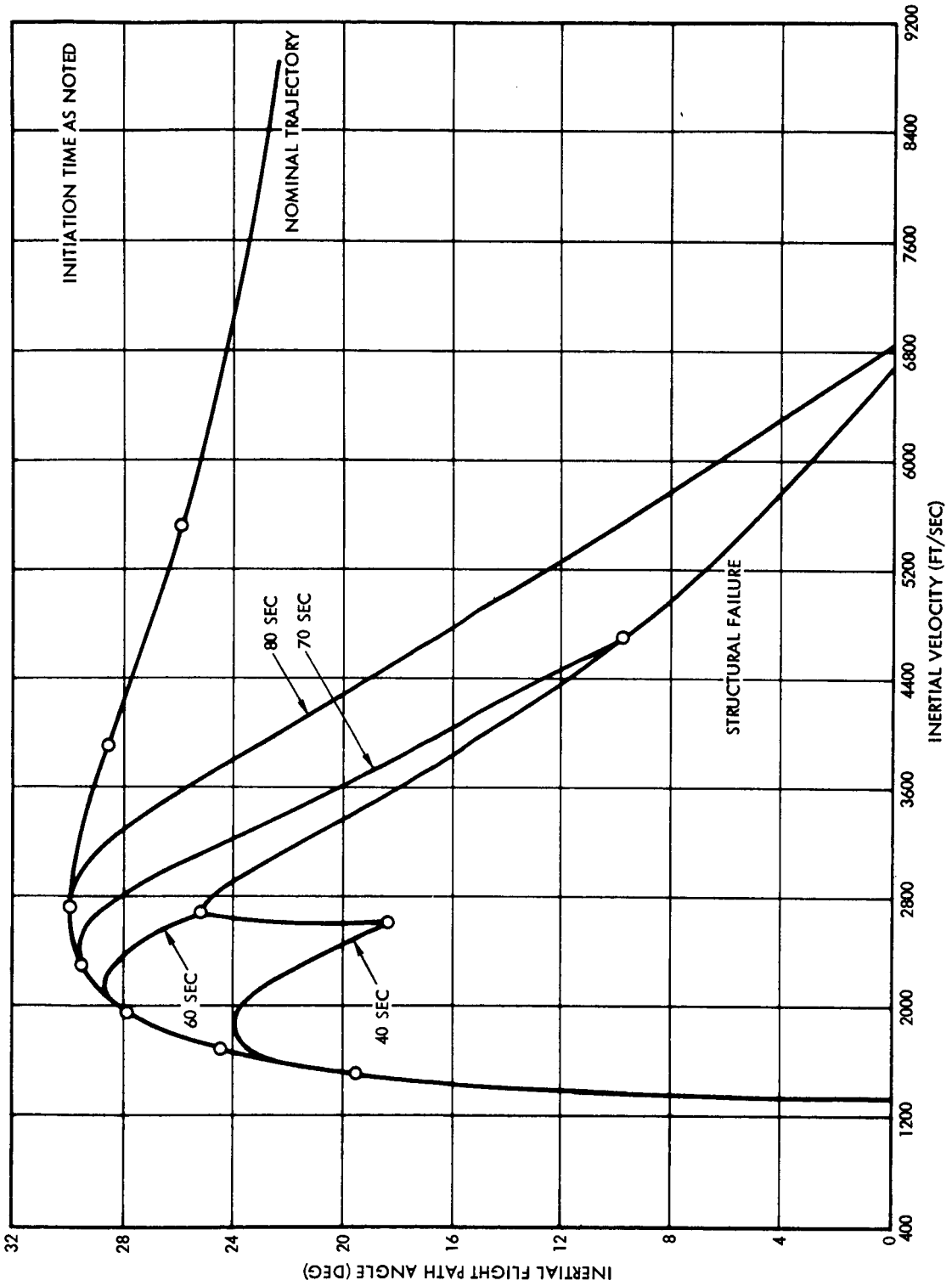

Figure 9. AS-503 Malfunctioning Gyro Trajectories, Constant 1.0 deg/sec Pitch Down Drift Rate with Delayed Initiation Times

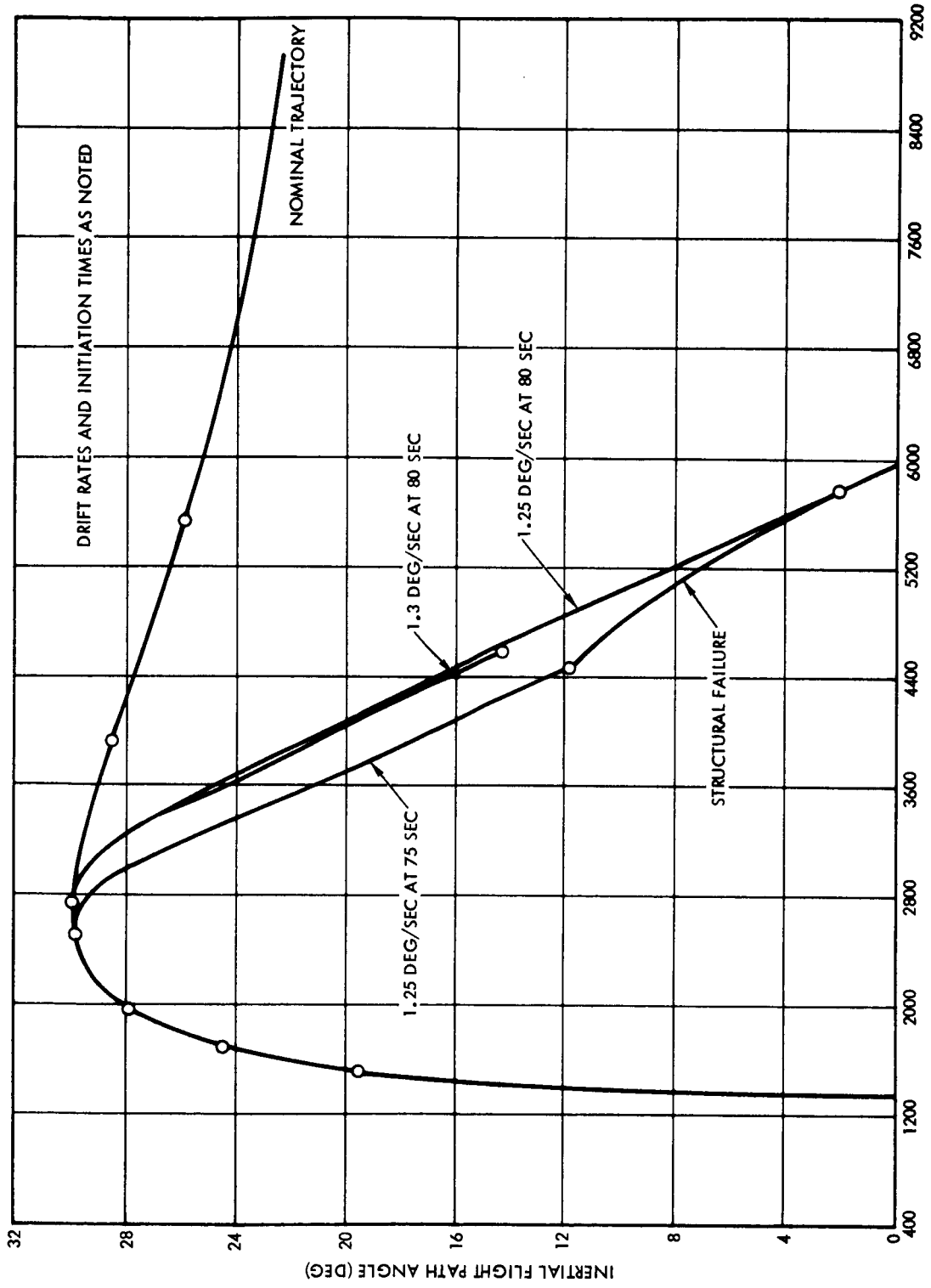

Figure 10. AS-503 Malfunctioning Gyro Trajectories, Constant Pitch Down Rates with Delayed Initiation Times

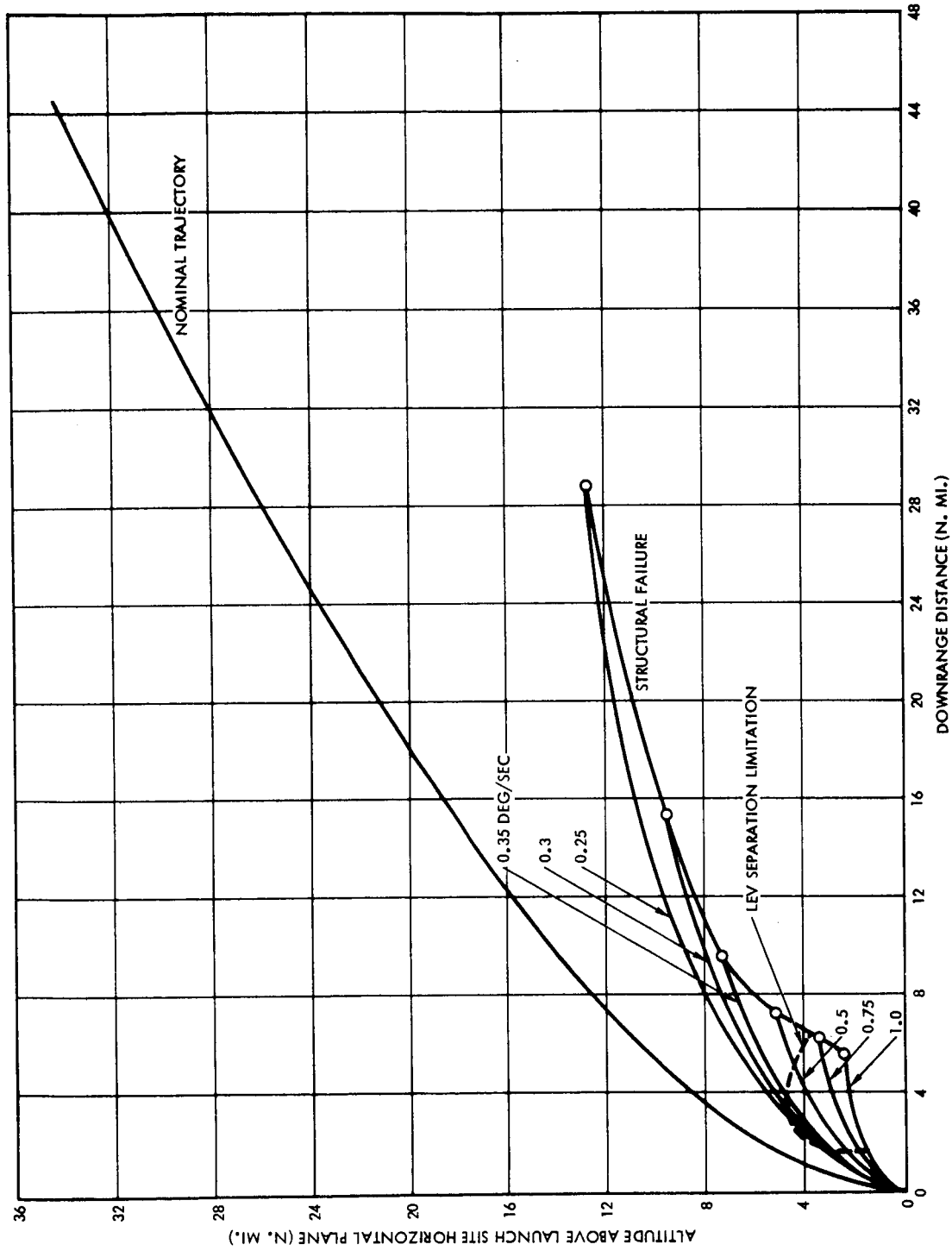

Figure 11. AS-503 Malfunctioning Gyro Trajectories, Constant Pitch Down Drift Rate Initiated at Lift-off

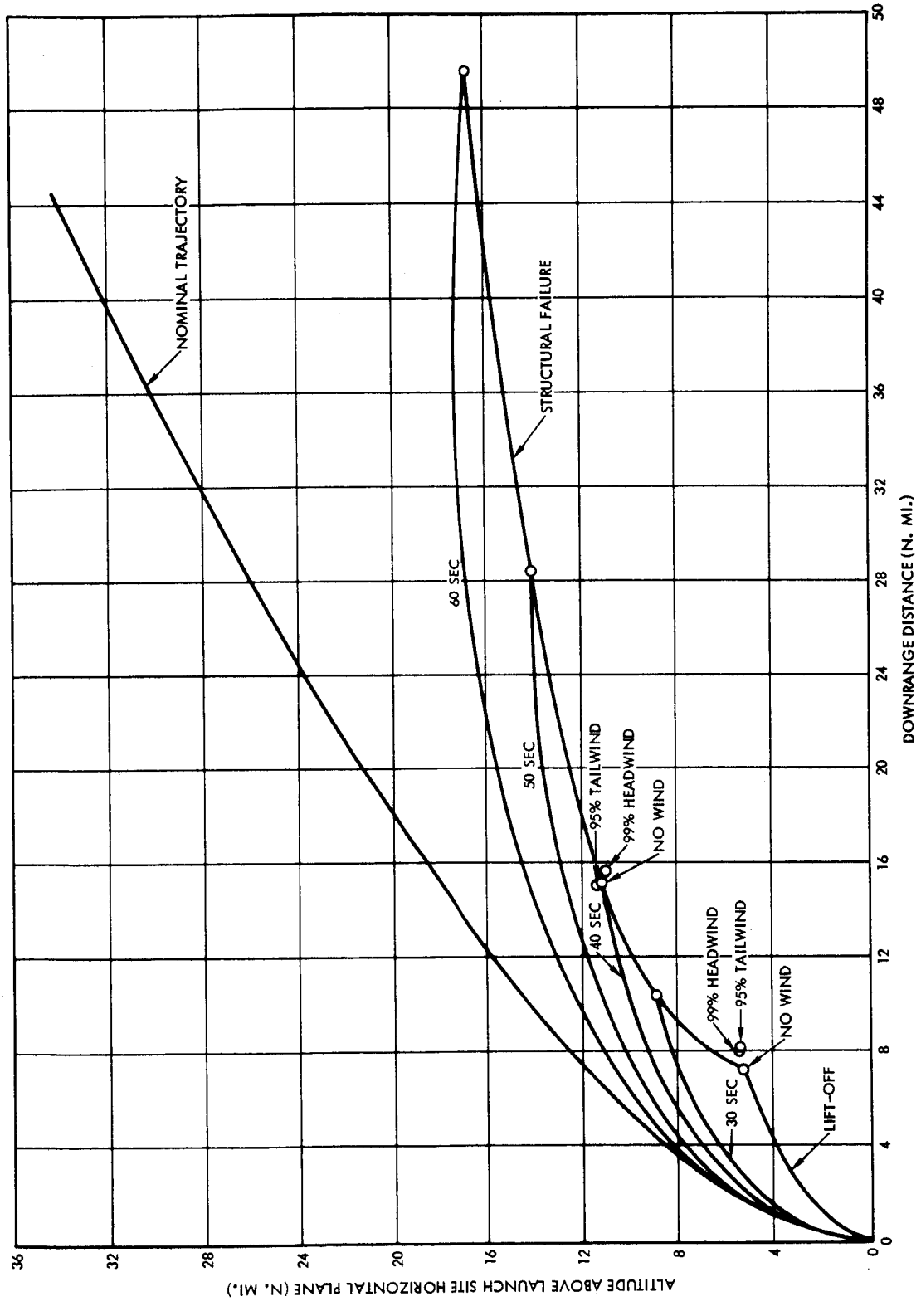

Figure 12. AS-503 Malfunctioning Gyro Trajectories, Constant 0.5 deg/sec Pitch Down Drift Rate with Delayed Initiation Times

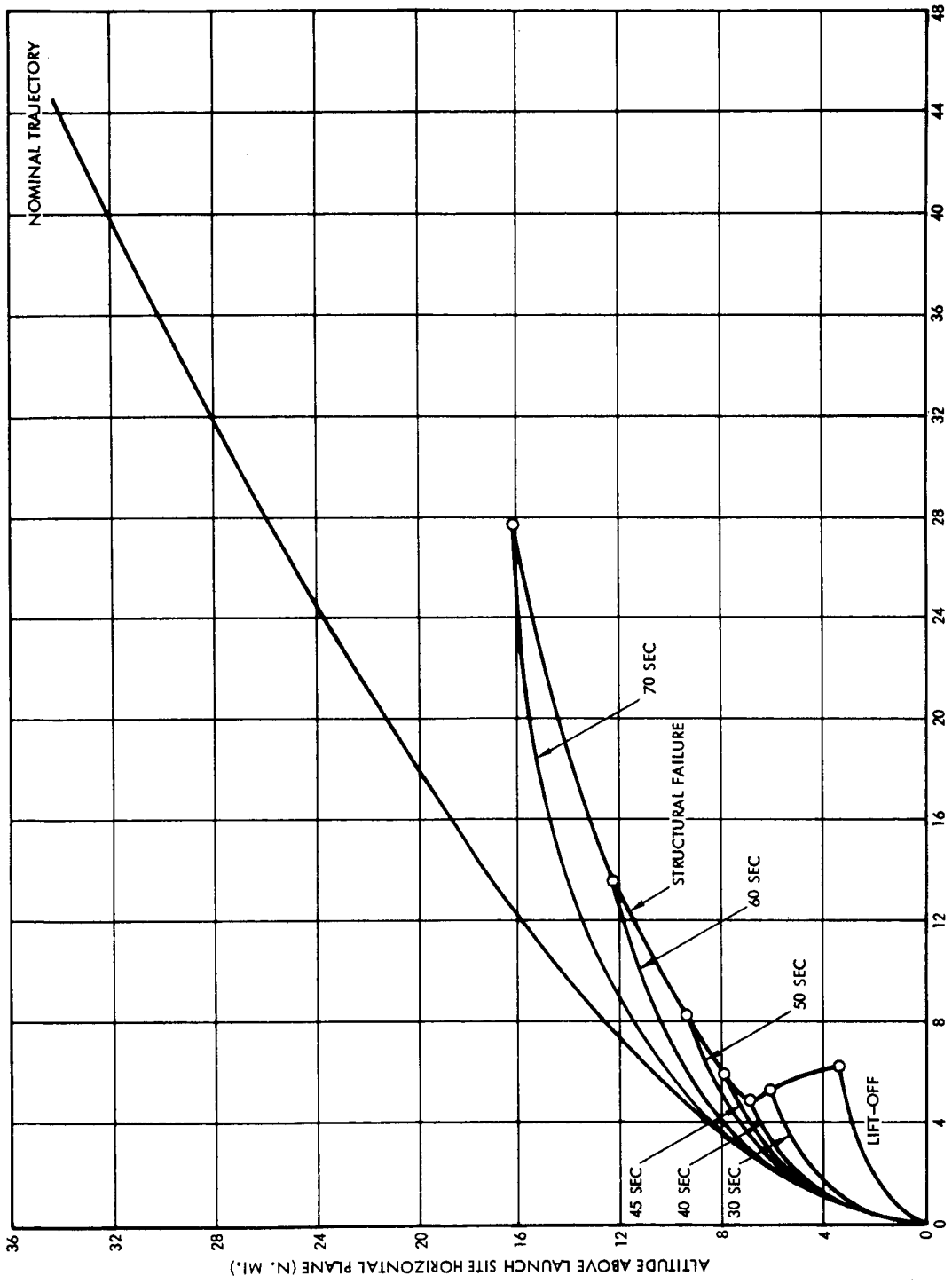

Figure 13. AS-503 Malfunctioning Gyro Trajectories, Constant 0.75 deg/sec Pitch Down Drift Rate with Delayed Initiation Times

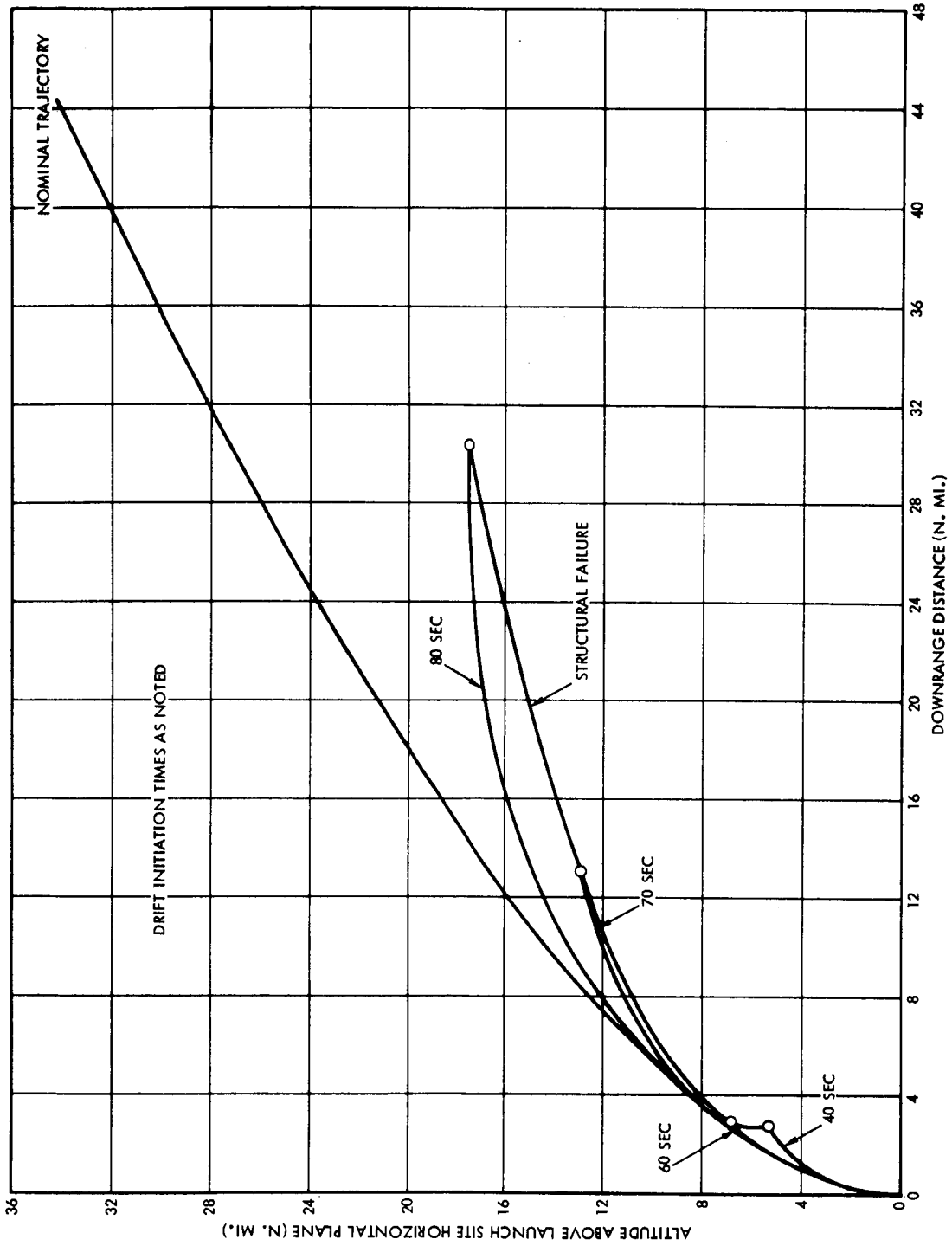

Figure 14. AS-503 Malfunctioning Gyro Trajectories, Constant 1.0 deg/sec Pitch Down Drift Rate with Delayed Initiation Times

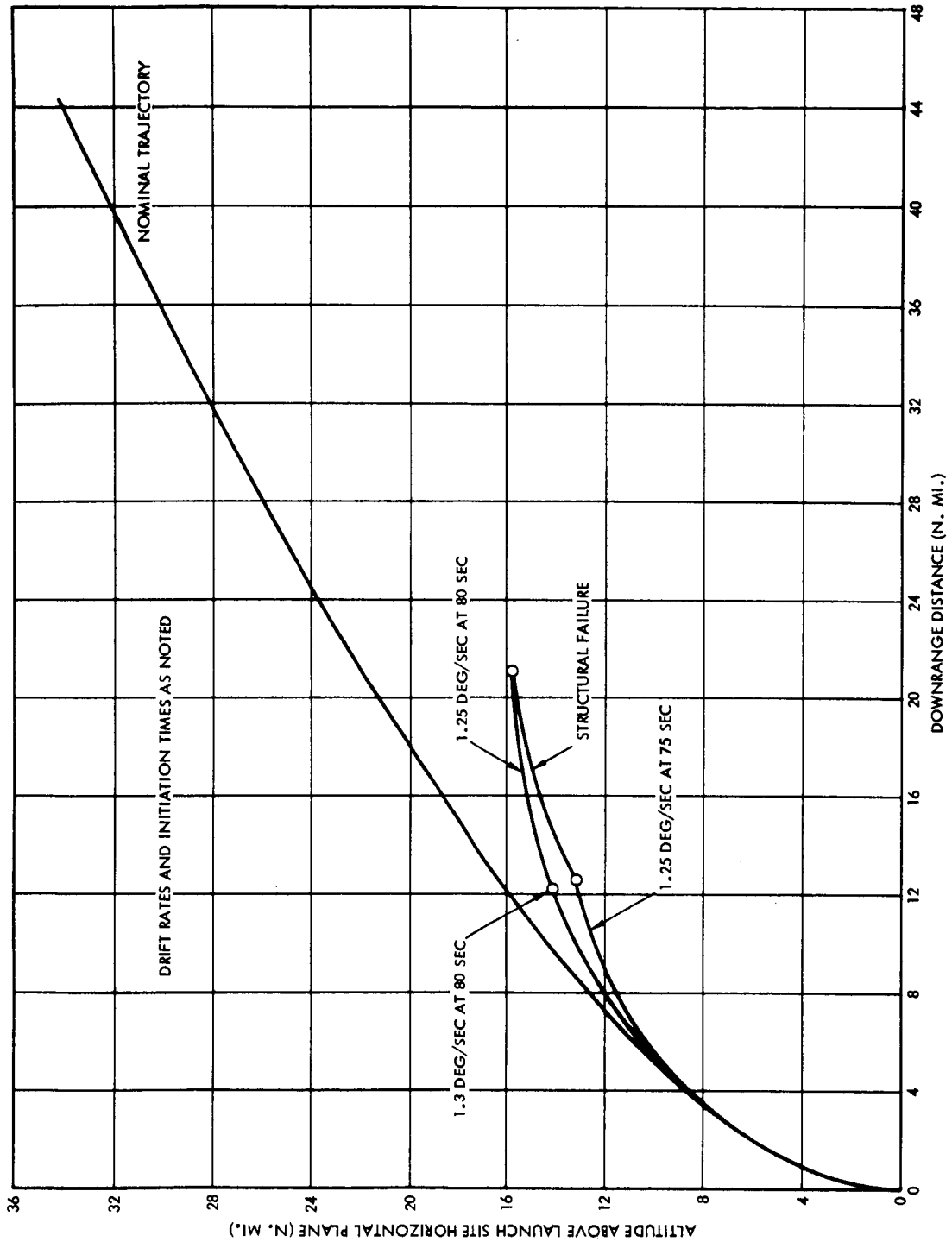

Figure 15. AS-503 Malfunctioning Gyro Trajectories, Constant Pitch Down Drift with Delayed Initiation Times

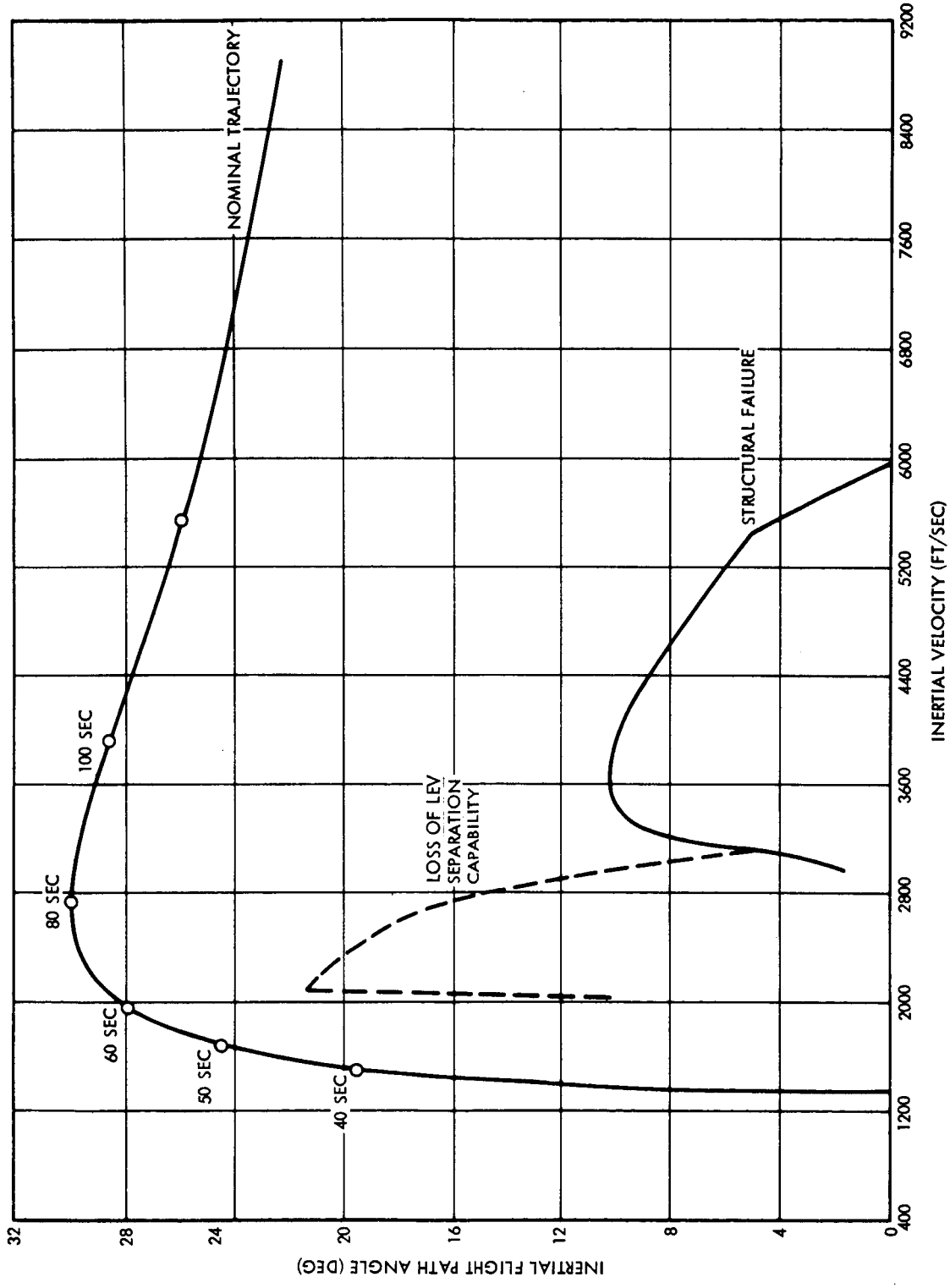

Figure 16. AS-503 Limit Lines

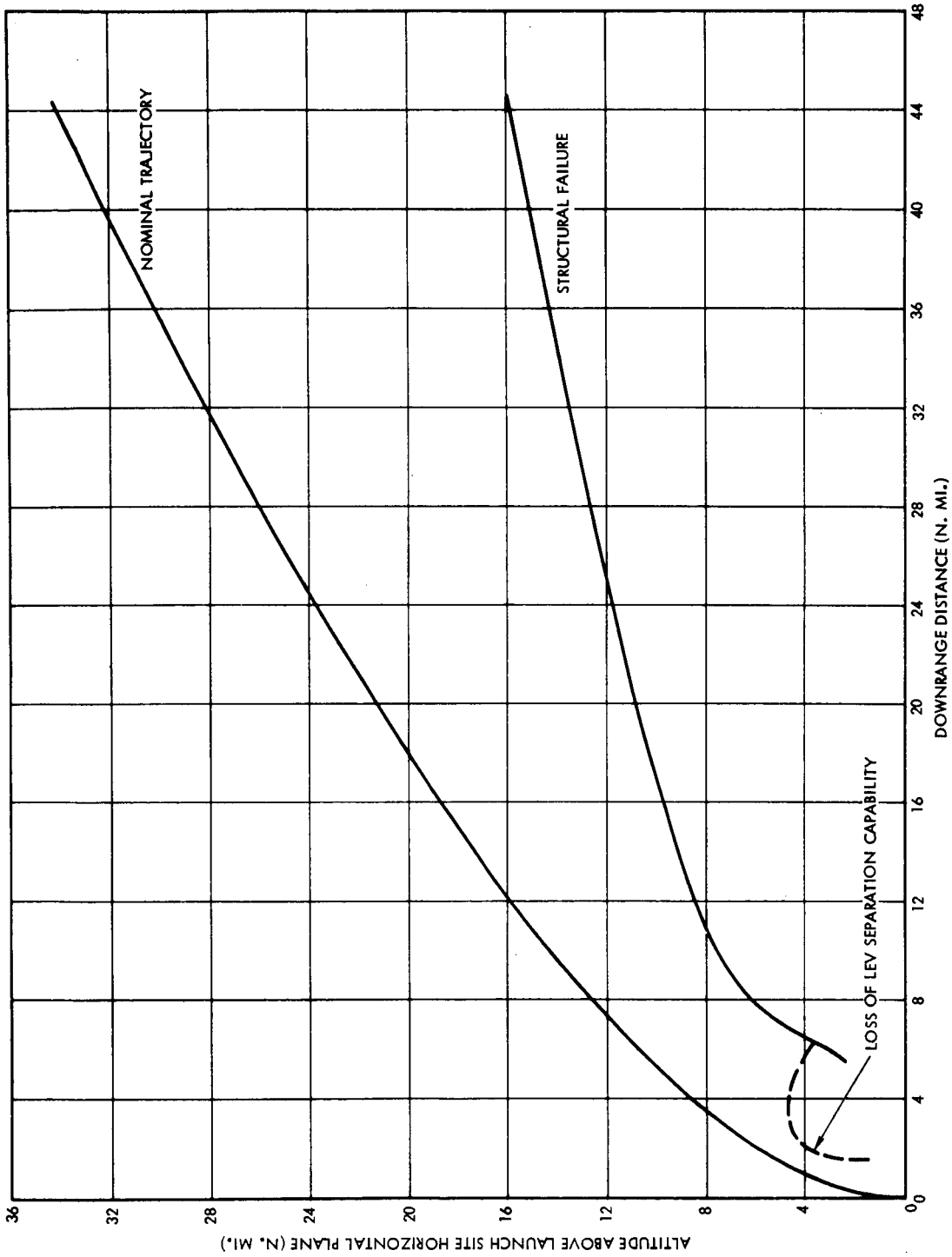

Figure 17. AS-503 Limit Lines

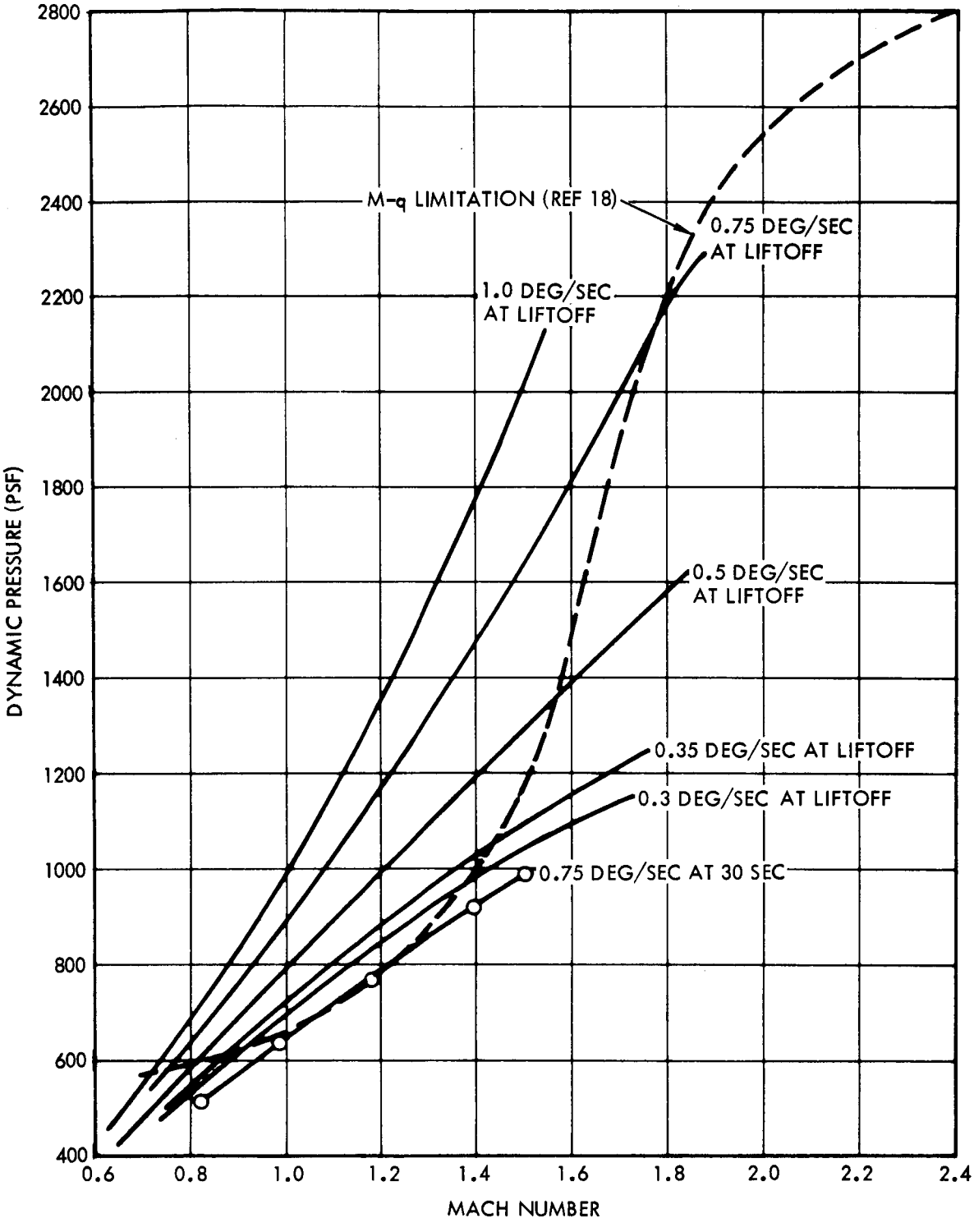

Figure 18. AS-503 LEV Separation Limitations

REFERENCES

1. "Abort Limit Lines Due to Saturn IB and Apollo Block I Structural Constraints," TRW 05952-6082-R000, 9 December 1966.

2. "Final Documentation of the Eighth Flight Limits Subpanel," NASA File No. 67-FM13-166, 1 June 1967.

3. "Directional Wind Component Frequency Envelopes, Cape Kennedy, Florida Atlantic Missile Range," NASA TMX 53009, 21 February 1964.

4. "Saturn V AS-503 Projected Mass Characteristics," MSFC R-P&VE-VAW-66-101, 19 October 1966.

5. "Apollo Mission Data Specification C, Apollo Saturn 503A (U)," TRW 2131-H006-R8-000 (C).

6. "Saturn V Design Mass Characteristics," MSFC R-P&VE-VAW-65-16, 5 February 1965.

7. "Static Aerodynamic Characteristics of the Apollo-Saturn V Vehicle," NASA TMX 53307, 26 July 1965.

8. "Generalized Forces for Apollo Spacecraft on Saturn V and Saturn IB," TRW Report 2251-6031-R0000, 1 May 1966.

9. "MTCP Task A-96 - Acquisition of Data During Subtask A-96.4," TRW 66-3342.2-65, 15 August 1966.

10. "Stabilization Networks for S-IC Stage Burn, Pitch and Yaw," MSFC R-ASTR-F-67-83, 22 March 1967.

11. "Patrick AFB Reference Atmosphere," 1963 Revision, NASA TMX 53139.

12. "AS-503 Launch Vehicle Reference Trajectory (U)," TBC Dγ-15480, 29 August 1966 (C).

13. Lyle Jenkins, "Transmittal of Apollo Spacecraft Structural Capability Data," MSC Letter to MSFC, 26 July 1965.

14. "Moment Versus Axial Load Data for Saturn IB and Saturn V Vehicle," MSFC R-P&VE-38-65-83, 28 October 1965.

15. "Request for Determination of Tensile Strength of S-II, S-IVB Stages and Instrument Unit Structural Joints for Vehicles AS-503 and Subsequent," MSFC R-P&VE-SS-67-15, 1 March 1967.

16. Telecon between M.E. White, TRW Systems and Wayne Holland, NASA/MSFC on 27 July 1966.

17. "Exit Heating Limits for AS-501," MSC 66-FM13-244, 27 July 1966.

18. "Task A-96.11 Launch Escape Vehicle Separation Limitations for Saturn V Launch Vehicles," TRW 3423.2-4, 2 June 1967.